

Dynamic Analysis of Frequency-Controlled Electronic Ballasts

Yan Yin, Regan Zane, Robert Erickson
Colorado Power Electronics Center
University of Colorado at Boulder
Boulder, CO 80309-0425

John Glaser
General Electrical Company
Global Research Center
One Research Circle
Niskayuna, NY 12309

Abstract—This paper presents analytical tools aimed at improving and simplifying the development of frequency-controlled dimming electronic ballasts. A modified phasor transformation is proposed that converts a frequency-modulated signal into an equivalent time-varying phasor. The proposed transformation is applied to develop a complete small-signal phasor model of the LCC resonant ballast, which explicitly models the effect of the frequency modulation on the envelopes of the outputs. A Spice-compatible implementation of the model is presented that facilitates AC analysis of the ballast in addition to envelope transient simulation, and is verified through comparison of experimental and simulation results. A closed-form solution of the control-to-output current transfer function for the ballast-resistor system is presented, along with key observations of the pole locations and low-frequency gain that facilitate simple and intuitive compensator design. Finally a design example for the feedback controller is given to verify the theoretical analysis.

Key Words—phasor transformation; frequency modulation; resonant ballast; small-signal phasor model

I. INTRODUCTION

With the growing demand for more intelligent and universal lighting products, there exists a significant need for improved analytical tools for the development of lighting electronic ballasts. This paper presents tools for analyzing the dynamic behavior of frequency-controlled dimming fluorescent ballasts, which aid the design of feedback controllers and give an intuitive understanding of the effects of component and load changes on the loop stability.

In many dimming ballast designs, a simple low-frequency (LF) feedback loop is employed to stabilize the lamp current and improve the crest factor. In practice, oscillations are frequently observed at low power levels, requiring additional design iterations and more complex feedback control. To predict and compensate for these phenomena, dynamic analysis of the control-to-output characteristics is needed. As shown in Fig. 1, the control input can be bus voltage variation (amplitude modulation, AM) or frequency variation (frequency modulation, FM), and the desired output is the resulting envelope variation in the lamp current. These issues were investigated and modeled using a time-varying phasor transformation in [1] for the special case of operation at resonance with AM, and in [2,3] a Spice model was developed

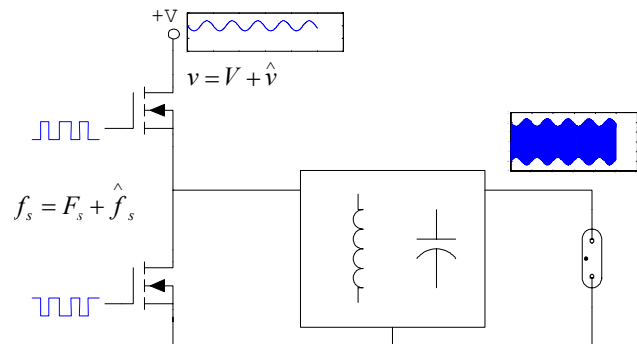


Fig. 1 High-frequency ballast driven by AM/FM input using the phasor transformation to enable envelope transient simulation of AM and phase modulation (PM).

This paper focuses on the dynamic analysis of the envelope behavior in the frequency-controlled ballast system. In Section II, a modified phasor transformation that converts an FM signal into an equivalent phasor is first proposed, and then is applied to derive the complete small-signal phasor model of the frequency-controlled dimming ballast, in which the effects of the frequency modulation on the envelopes of the output current/voltage are explicitly modeled. In Section III a Spice-compatible small-signal model is developed for Spice AC analysis, and is verified by the measurements. Section IV gives a closed-form solution of the frequency-to-output current transfer function of the small-signal ballast model with the resistive load, along with key observations of the pole locations and LF gain that facilitate simple and intuitive solution of the transfer function. The effects of the negative incremental impedance of the fluorescent lamp [1] on the dynamics of the studied LCC ballast system are also discussed. Section V presents a feedback controller design example. The conclusions are summarized in Section VI.

II. MODIFIED PHASOR TRANSFORMATION AND ITS APPLICATION TO THE FREQUENCY-CONTROLLED BALLAST

The object in performing the phasor transformation is to remove the switching frequency components of the sinusoidal waveforms and analyze the dynamics of the signal envelopes. For the typical half-bridge ballast, the sinusoidal approximation can be applied as long as the converter operates near

resonance with high Q-factor [4]. The transformation approach was first proposed in [5], where a sinusoidal signal can be represented by a complex phasor:

$$x(t) = \text{Re}[\bar{x}(t)e^{j\omega_s t}], \quad (1)$$

where $\bar{x}(t)$ is the time-varying phasor corresponding to $x(t)$. This transformation approach is well suited to small-signal modeling of amplitude modulation, where the switching frequency ω_s is constant. Small variations in the amplitude of $x(t)$ are then modeled by small variations in $\bar{x}(t)$. Hence a small-signal time-invariant phasor model can be derived. However, frequency modulation causes $\bar{x}(t)$ to contain a rotating component. The variations in $\bar{x}(t)$ are no longer small, and small-signal analysis cannot be applied.

To accommodate frequency modulation, we need to consider a time varying frequency $\omega_s(t)$. Based on the definition of frequency modulation (assuming the carrier is sinusoidal)

$$x_{FM}(t) = A \cos\left(\int \omega_s(t) dt\right), \quad (2)$$

we propose a modified phasor transformation of the form

$$x(t) = \text{Re}[\bar{x}(t)e^{j\int \omega_s(t) dt}]. \quad (3)$$

This proposed new approach is useful for small-signal modeling when $x(t)$ contains both amplitude and frequency modulation. Frequency modulation no longer leads to a rotating component in $\bar{x}(t)$. Small variations in the amplitude of $x(t)$ lead to small variations in $\bar{x}(t)$, which satisfies the small-signal assumption.

By applying (3) to the basic circuit element v - i equations, we can get the large-signal phasor models for these circuit elements as shown in Fig. 2. As an example, we apply (3) to the differential equation of the inductor to demonstrate how to get the phasor model. The v - i equation of the inductor is

$$L \frac{di(t)}{dt} = v(t). \quad (4)$$

The phasor transformations of current and voltage are:

$$i(t) = \text{Re}[\bar{i}(t)e^{j\int \omega_s(t) dt}] \quad (5)$$

$$v(t) = \text{Re}[\bar{v}(t)e^{j\int \omega_s(t) dt}]$$

Upon application of (5) to (4), the phasor equation for the inductor is obtained:

$$L \frac{d\bar{i}(t)}{dt} + j\omega_s(t)L\bar{i}(t) = \bar{v}(t). \quad (6)$$

Equation (6) can be converted to a circuit model as an inductor in series with an imaginary resistor, as shown in Fig. 2. Through a similar approach, the large-signal phasor models for an FM voltage source, resistor and capacitor can also be obtained. These models are similar to those in [5], except that here the imaginary resistors can be time varying.

To derive the small-signal phasor models, we need to perturb and linearize the large-signal phasor models. With the assumption that:

$$\bar{v} = \bar{V} + \hat{v}, \quad \bar{i} = \bar{I} + \hat{i}, \quad \text{and} \quad \omega_s = \Omega_s + \hat{\omega}_s,$$

then the small-signal phasor model for the inductor is obtained as:

$$L \frac{d\hat{i}}{dt} + j\Omega_s L \hat{i} + j\hat{\omega}_s L \bar{I} = \hat{v}. \quad (7)$$

Similarly, the small-signal phasor models for other circuit elements can be derived. They are also shown in Fig. 2.

The phasor model of any resonant topology can then be found by simply replacing the basic elements according to Fig. 2. Fig. 3 shows the small-signal phasor model for a typical LCC resonant ballast with the lamp initially modeled as a resistor.

It is notable that in the small-signal phasor model shown in Fig. 3, the effect of frequency modulation on the resonant tank is explicitly modeled as dependent sources that are associated with each reactive element (voltage source with inductor and current source with capacitor). These dependent sources alter the output phasors, resulting the amplitude modulation of the time-domain signals. Hence the FM input, after passing through the reactive network, is converted to an AM/FM output.

Once the phasor of any signal is obtained by solving the phasor model, the original signal envelope can be recovered

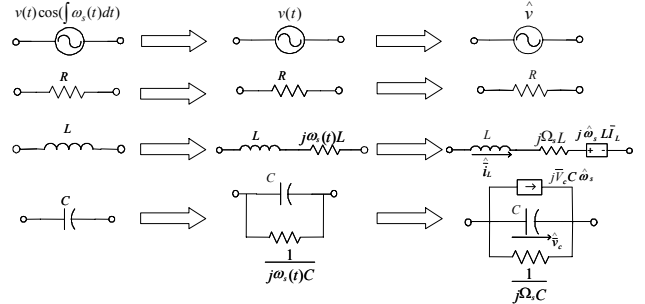


Fig. 2 Large-signal and small-signal phasor models for basic circuit elements

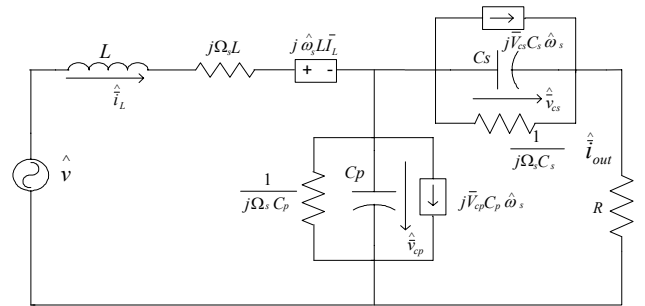


Fig. 3 Small-signal phasor model for LCC ballast

by finding the magnitude of the phasor [2,3]:

$$x_{en}(t) = |\bar{x}(t)| = \sqrt{x_1^2(t) + x_2^2(t)}, \quad (8)$$

where $x_1(t)$ and $x_2(t)$ are the real and imaginary part of $\bar{x}(t)$, respectively.

By perturbing and linearizing (8), we can find the small signal variation of the envelope as:

$$\hat{x}_{en} = \frac{X_1 \hat{x}_1 + X_2 \hat{x}_2}{\sqrt{X_1^2 + X_2^2}} = \frac{X_1 \hat{x}_1 + X_2 \hat{x}_2}{X}, \quad (9)$$

where X_1 , X_2 and X are steady-state values of the real part, imaginary part and magnitude of the phasor, \hat{x}_1 and \hat{x}_2 are the small signal components of the real and imaginary part of the phasor.

III. SPICE-COMPATIBLE MODEL AND EXPERIMENTAL VERIFICATION

Owing to the existence of imaginary resistors, the model in Fig. 3 cannot be directly realized in a Spice-compatible simulator. However, by use of the same approach presented in [2], this complex circuit can be split into real and imaginary part, as shown in Fig. 4, and implemented in a Spice simulator for transient and AC analysis.

Fig. 5 compares the transient simulation result for an FM input ($\hat{\omega}_s$ is set to a sinusoidal signal) with the original time-domain waveform (only the positive portion is shown here). It can be seen that the phasor model gives exactly the envelope of the original time-domain waveform without switching level simulation.

The model in Fig. 4 can also be implemented in Spice for AC analysis to find any transfer function corresponding to input voltage (\hat{v}) or frequency ($\hat{\omega}_s$ or \hat{f}_s). Then the simulation results can be compared with the measurements. Fig. 6 shows the experimental setup for the measurement of the transfer function of frequency-to-output current. The voltage-controlled oscillator (VCO) is used to generate the frequency modulation. The switching frequency is then controlled by the VCO input voltage with

$$F_s + \hat{f}_s = k_{VCO}(V_b + \hat{v}_f). \quad (10)$$

The input filter of the network analyzer filters all the high-frequency components in v_{sen} and only the component with the modulating frequency is measured. Hence, the measured transfer function is proportional to the transfer function from frequency to output current envelope $\hat{i}_{out_en}/\hat{f}_s$.

Fig. 7 compares PSpice simulation and experimental results of the frequency-to-output current transfer function with $F_s = 100\text{kHz}$, $R = 300\Omega$ and $k_{VCO} = 20\text{kHz/Volt}$. It can be seen that the simulation result is in good agreement with the measurement.

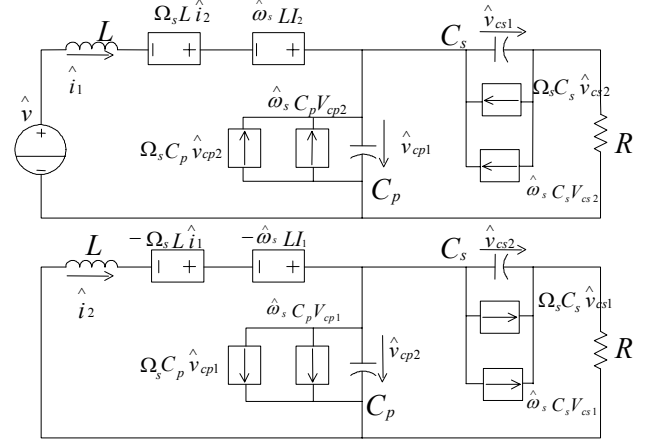


Fig. 4 Spice-compatible small-signal phasor model for LCC ballast

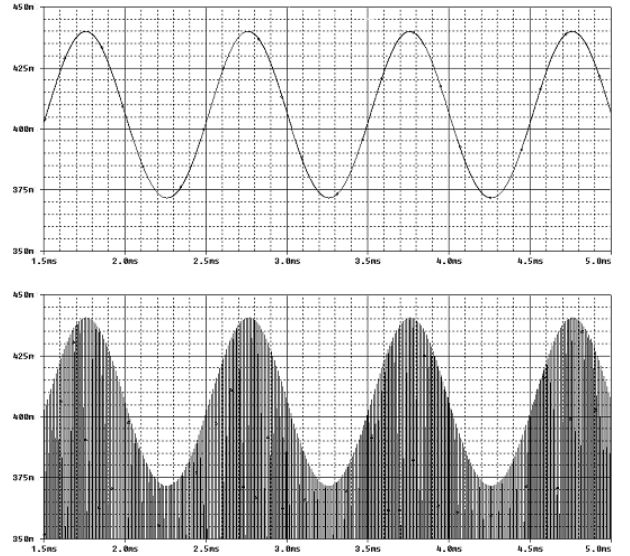


Fig. 5 Transient analysis given by the phasor model (top) and the original LCC ballast

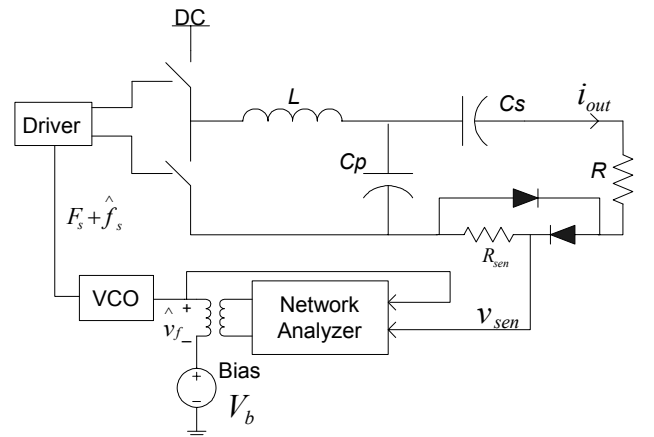


Fig. 6 Experimental setup for control-to-output current transfer function measurement ($L=539\mu\text{H}$, $C_s=4.3\text{nF}$, $C_p=3.8\text{nF}$)

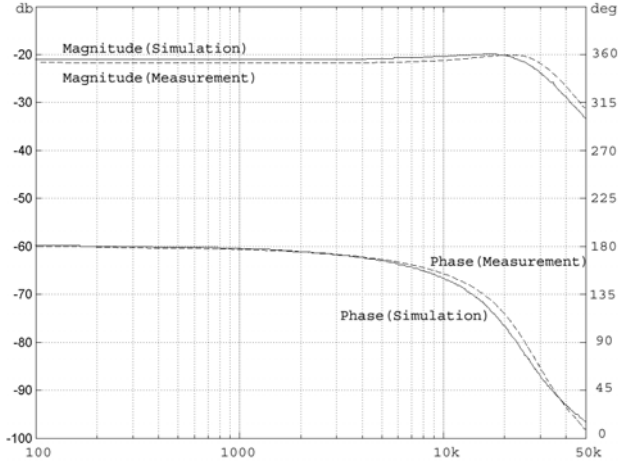


Fig. 7 Simulation and measurement results of frequency-to-output current transfer function with resistive load $R=300\Omega$

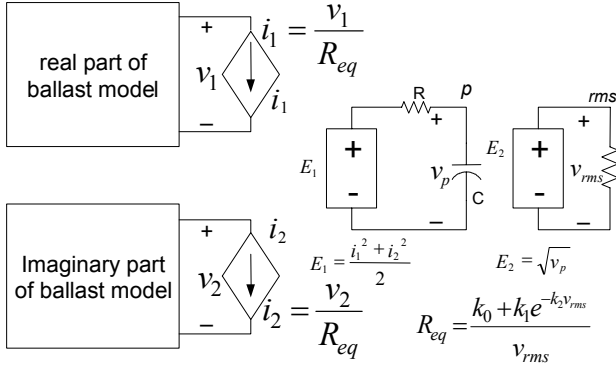


Fig. 8 Spice model combining the ballast model with the fluorescent lamp model

In the discussion above, the simulation and experimental results are found based on the resistive load in order to verify the theoretical phasor model for the ballast. To model the dynamic envelope behavior of the ballast-fluorescent lamp system, the lamp model should be incorporated into the ballast model using the approach similar to [3], as shown in Fig. 8. The lamp model shown in Fig. 8 is similar to the one in [3] except the polynomial curve fitting is replaced by the exponential function. The simulation and experimental results are compared in Fig. 9, where a GE Biax™ 26W compact fluorescent lamp (CFL) is used as the load with operating frequency $F_s = 100\text{kHz}$ and $P_{lamp} = 24\text{W}$. Again, there is good agreement between the simulation and measurement results.

IV. ANALYSIS

The Spice models of Section III facilitate AC simulation of dimming ballasts, but still lack intuitive aids useful for the development of ballast systems. In this section, we highlight a few key observations from the theoretical analysis that give a more intuitive feel for the system operation.

By combining the reactive elements with their corresponding imaginary resistors in Fig. 3, we can find that in the

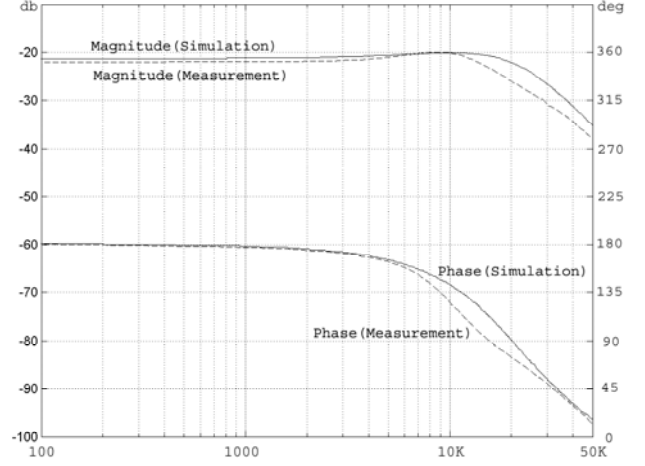


Fig. 9 Simulation and measurement results of frequency-to-lamp current transfer function with a GE Biax™ 26W CFL ($P_{lamp}=24\text{W}$)

S -domain the resulting small-signal model topology is similar to that of the original LCC resonant tank except that $s + j\Omega_s$ replaces s . The similarity in the topology means that the small-signal model in Fig. 3 has the same denominator as the resonant tank except that the variable s is replaced by $s + j\Omega_s$.

Upon solving the model in Fig. 3, the transfer function from frequency to output current phasor can be manipulated into the following closed-form:

$$G_{f-ph}(s) = \frac{\hat{i}_{out}}{\hat{f}_s} = \frac{N(s + j\Omega_s)}{D(s + j\Omega_s)} = \frac{N(s + j\Omega_s)D(s - j\Omega_s)}{D(s + j\Omega_s)D(s - j\Omega_s)} = G_{f-ph_{re}}(s) + jG_{f-ph_{im}}(s) \quad (11)$$

where $D(s)$ represents the characteristic equation of the original LCC tank, and $N(s)$ is a second order polynomial. Then, according to (9), the transfer function from frequency to output current envelope can be expressed as:

$$G_f(s) = \frac{\hat{i}_{out_{en}}}{\hat{f}_s} = \frac{1}{\sqrt{I_{out1}^2 + I_{out2}^2}} (I_{out1}G_{f-ph_{re}}(s) + I_{out2}G_{f-ph_{im}}(s)) \quad (12)$$

where I_{out1} and I_{out2} are the steady-state real and imaginary part of the output current phasor, respectively.

Although the resulting closed-form solution is an intimidating sixth-order transfer function, when put in the form of (11) and (12), it can be seen that the poles of the system are simply the poles of the original LCC tank shifted up and down by $j\Omega_s$. The pole diagram for a typical LCC ballast is shown in Fig. 10, where “*” represents the poles of the LCC resonant tank, and “Δ” represents the poles of the small-signal model. As the ballast is generally operated near and above the resonant frequency, this creates a pair of complex poles at low frequency (ω_1 in Fig. 10), which dominate the open-loop response over the bandwidth of a

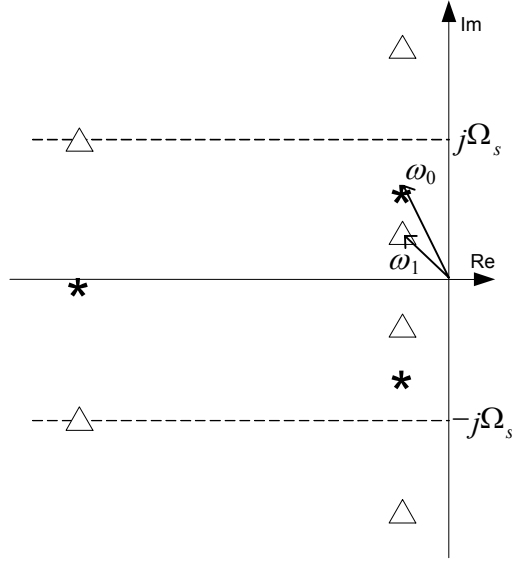


Fig. 10 Poles of the LCC resonant tank and the small-signal phasor model

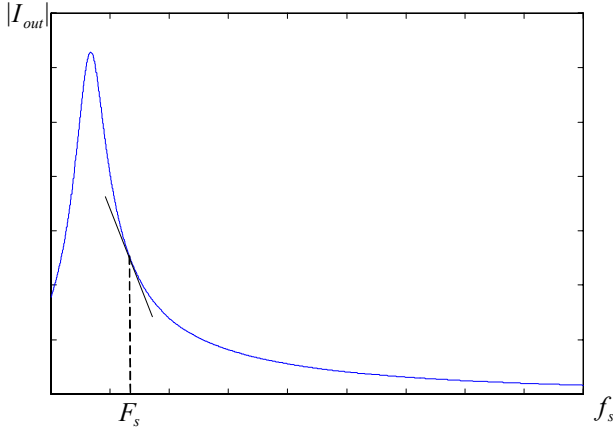


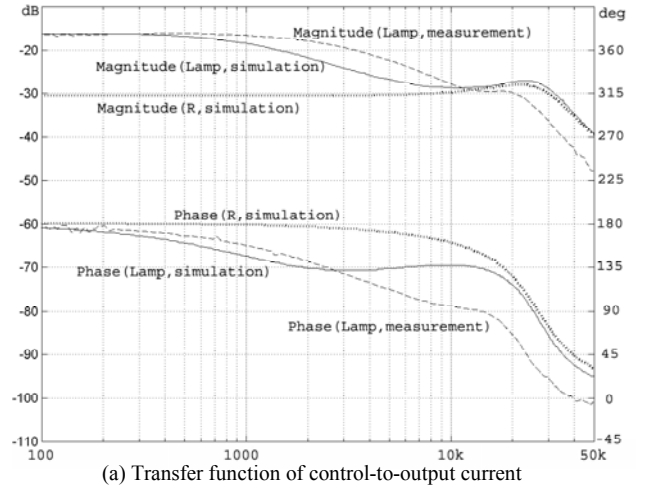
Fig. 11 LF gain of the small-signal phasor model for LCC ballast

typical feedback controller. From Fig. 10, ω_1 can be determined as

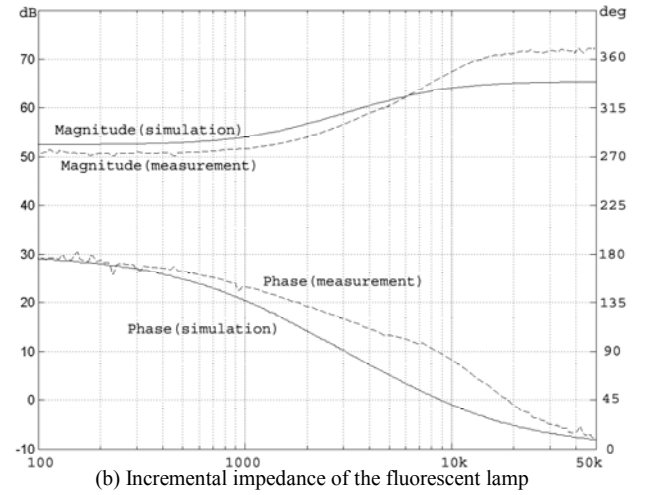
$$\omega_1 = \sqrt{\Omega_s^2 - 2\Omega_s\omega_0\sqrt{1-1/(4Q^2)} + \omega_0^2}, \quad (13)$$

where ω_0 and Q are the resonant frequency and quality factor of the resonant tank. Approximately, if the ballast operates with high Q -factor, ω_1 can be estimated as $\Omega_s - \omega_0$. This approximation is in agreement with the argument in [6]. Other high-frequency (HF) poles, in general, can be ignored from the controller design point of view.

The LF gain of the transfer function can also be determined from the closed-form solution, although it may be even simpler to determine the LF gain directly from the steady-state solution of the ballast by finding the slope of the curve of output current magnitude vs. switching frequency evaluated at the quiescent operating frequency, as shown in Fig. 11 for the LCC ballast,



(a) Transfer function of control-to-output current



(b) Incremental impedance of the fluorescent lamp

Fig. 12 Simulation and measurement results for LCC ballast with GE Biax™ 26W CFL at low dimming level (30% of the full power)

$$G_0 = \left. \frac{\partial |I_{out}|}{\partial f_s} \right|_{f_s = F_s}. \quad (14)$$

While the above analysis is based on the resistive load, for more accurate results, the dynamics of the fluorescent lamp should be taken into account to obtain the complete dynamics of the ballast system. As seen by comparing Figs. 7 & 9, the dynamics of the lamp have negligible effect on the system dynamics at high power levels, which is a key assumption in most non-dimming ballast designs. However, as seen in Fig. 12(a), the actual transfer function with a lamp load can deviate significantly from the resistive load assumption at low dimming levels. For the LCC ballast system being measured, it can be seen that an additional LF pole/zero pair come into the transfer function with the fluorescent lamp load, which alter the LF gain and phase shift and complicate the controller requirements. We believe that the increased effects of the lamp on the system at low dimming levels can be intuitively understood by noting the significantly reduced output impedance of the ballast and increased effective impedance of the lamp. It should be noted that the deviation between

measurement and simulation is more pronounced at low dimming levels (compare Fig. 9 & 12(a)) due to non-idealities of the lamp model, which can be seen by comparing the simulated and measured incremental impedance of the fluorescent lamp in Fig. 12(b). To obtain more accurate simulation results, a higher order lamp model and more complicated curve fitting could be used.

In order to account for the dynamics of the lamp analytically, a small-signal phasor model of the lamp would need to be developed to replace the resistive load in Fig. 3, which could then be solved and manipulated into the forms similar to (11) and (12). While this may be included in our future work, at this point it appears that such an exercise will result in a transfer function that can only be solved numerically, providing little insight into the system operation. We are currently pursuing alternative analysis approaches or extensions that may facilitate generalized analytical results for the complete lamp-ballast system.

Although we do not yet have complete analytical results, we can make a few key observations from the above analysis regarding the effects of the lamp on the dynamics of this LCC ballast topology (Fig. 6) at low dimming levels:

- The LF pole and zero in the transfer function nearly match the zero and pole in the incremental impedance of the fluorescent lamp, respectively.
- The lamp mainly affects the system dynamics in the LF range. For HF perturbation, the lamp behaves essentially like a pure resistor.

Based on the above results, we can define a suitable feedback controller design procedure for the dimming LCC ballast as follows:

- 1) Determine the LF gain and the frequency of the double poles of the frequency-to-output current transfer function from the phasor ballast model (with equivalent resistive load).
- 2) Select the crossover frequency well below the frequency of the double poles.
- 3) Determine the magnitude and phase effects of the lamp on the system at low dimming levels from the simple measurement of incremental impedance of the fluorescent lamp.
- 4) Design the compensator to achieve high LF gain, desired crossover frequency and phase margin.

V. FEEDBACK CONTROLLER DESIGN EXAMPLE

In this section, we present a design example of the feedback controller for the LCC ballast shown in Fig. 13 with GE Biax™ 26W CFL according to the dynamic analysis and discussion in the previous sections.

A typical compensator is the simple integrator as

$$G_c(s) = \frac{2\pi f_0}{s} \quad (15)$$

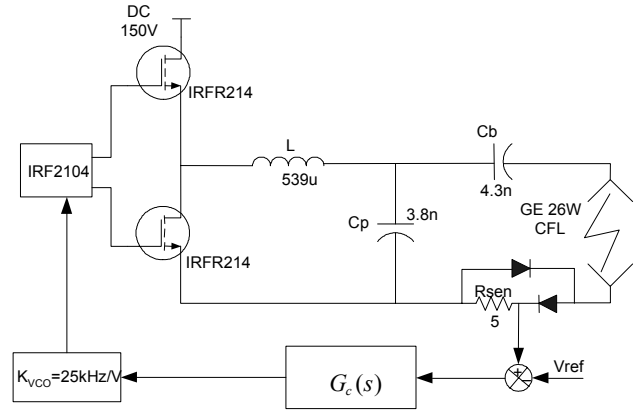
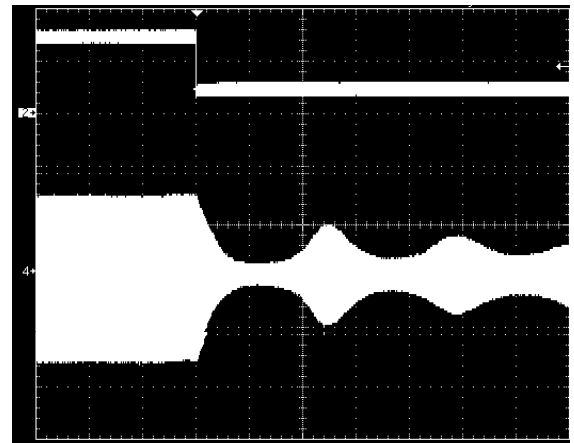


Fig. 13 Closed-loop system of LCC ballast with GE Biax™ 26W CFL



upper trace: current reference 100mV/div
lower trace: lamp current 50mA/div
time: 400us/div

Fig. 14 Step response of the lamp current at low dimming levels with the integrator

with $f_0 = 2122\text{Hz}$ to achieve high LF gain and desired crossover frequency. This controller works well at high power levels, but some oscillation may occur at low dimming levels as shown in Fig. 14, where the lamp power is stepped from 30% to 15% of full power.

By following the procedure in the previous section, we can easily design a new compensator to obtain better performance:

- 1) From the phasor model, we know the LF gain of the frequency-to-output current transfer function (with the gains of the VCO and current sensor) is below -5dB and the frequency of the double pole is above 10kHz.
- 2) Select the crossover frequency around 1kHz for full power operation.
- 3) The zero and pole of the incremental impedance of the lamp are about 1 kHz and 10kHz, respectively, and the gain difference between LF and HF is about 15~20dB.
- 4) From the information given by step 1 to 3, we can choose the compensator as the following form

$$G_c(s) = \frac{2\pi f_1}{s} \frac{1 + \frac{s}{2\pi f_z}}{1 + \frac{s}{2\pi f_p}} \quad (16)$$

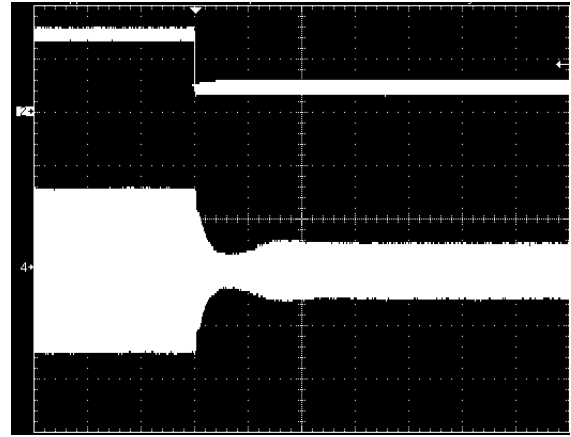
with $f_1 = 2122\text{Hz}$, $f_p = 3386\text{Hz}$, $f_z = 723\text{Hz}$.

Fig. 15 shows the step response of lamp current (from 80mA to 30mA in peak value) for this design at low dimming levels (from 30% to 15% of the full power). It can be seen that the system is stable as predicted.

VI. CONCLUSION

Studies of the dynamic behavior of the envelope signals are important for the development of the lighting electronic ballast. For dimming ballasts, frequency control is a significant case. In this paper, analytical tools are presented that are useful for dynamic analysis of frequency-controlled dimming electronic ballasts and development of feedback compensation networks.

A small-signal phasor model is presented for AC analysis of the effects of the frequency modulation on the lamp current envelope based on a modified phasor transformation by converting an FM signal into an equivalent time-varying phasor. The good agreement between the simulation results and measurements shows that this model can accurately predict the envelope dynamics. To aid development, key observations are presented that give intuitive analytical results on the LF gain and pole locations of the control-to-output current transfer function for the ballast-resistor system. The effects of the incremental impedance of the fluorescent lamp on the LCC ballast system dynamics at low dimming levels are also discussed. Based on these analytic and experimental results, a feedback controller design procedure for the studied LCC ballast system is proposed and a design example is given. The experimental result verifies that this controller works very well, even at very low dimming level.



upper trace: current reference 100mV/div
lower trace: lamp current 50mA/div
time: 400us/div

Fig. 15 Step response of the lamp current at low dimming levels with the PID compensator

REFERENCES

- [1] E. Deng, "1. Negative Incremental Impedance of Fluorescent Lamp", Ph.D. Thesis, California Institute of Technology, Pasadena, 1995.
- [2] S. Ben-Yaakov, S. Glozman, and R. Rabinovici, "Envelope Simulation by SPICE-Compatible Models of Linear Electric Circuits Driven by Modulated Signals," IEEE Trans. on Ind. Appl., Vol. 37, No.2, March/April. 2001, pp 527-533.
- [3] S. Glozman and S. Ben-Yaakov, "Dynamic Interaction Analysis of HF Ballasts and Fluorescent Lamps Based on Envelope Simulation," IEEE Trans. on Ind. Appl., Vol. 37, No.5, September/October. 2001, pp 1531-1536.
- [4] R. Erickson, D. Maksimovic, *Fundamentals of Power Electronics, second edition*, Massachusetts: Kluwer Academic Publishers, 2000.
- [5] C. T. Rim and G. H. Cho, "Phasor Transformation and its Application to the DC/AC Analyses of Frequency Phase-Controlled Series Resonant Converters (SRC)," IEEE Trans. on Power Electronics, Vol.5, No.2 April 1990, pp 201-211.
- [6] V. Vorperian, "Approximate Small-Signal Analysis of the Series and the Parallel Resonant Converters," IEEE Trans. on Power Electronics, pp 15-24.